

# Flux-pumped impedance-engineered broadband Josephson parametric amplifier

Cite as: Appl. Phys. Lett. **118**, 142601 (2021); <https://doi.org/10.1063/5.0035945>

Submitted: 01 November 2020 • Accepted: 25 March 2021 • Published Online: 09 April 2021

 J. Grebel,  A. Bienfait,  É. Dumur, et al.



View Online



Export Citation



CrossMark

## ARTICLES YOU MAY BE INTERESTED IN

[A quantum engineer's guide to superconducting qubits](#)

Applied Physics Reviews **6**, 021318 (2019); <https://doi.org/10.1063/1.5089550>

[Broadband parametric amplification with impedance engineering: Beyond the gain-bandwidth product](#)

Applied Physics Letters **107**, 262601 (2015); <https://doi.org/10.1063/1.4939148>

[Flux-driven Josephson parametric amplifier](#)

Applied Physics Letters **93**, 042510 (2008); <https://doi.org/10.1063/1.2964182>

 QBLOX



1 qubit

Shorten Setup Time

**Auto-Calibration**

**More Qubits**

Fully-integrated

**Quantum Control Stacks**

**Ultrastable DC to 18.5 GHz**

Synchronized <<1 ns

Ultralow noise



100s qubits

[visit our website >](#)



# Flux-pumped impedance-engineered broadband Josephson parametric amplifier

Cite as: Appl. Phys. Lett. **118**, 142601 (2021); doi: [10.1063/5.0035945](https://doi.org/10.1063/5.0035945)

Submitted: 1 November 2020 · Accepted: 25 March 2021 ·

Published Online: 9 April 2021



View Online



Export Citation



CrossMark

J. Grebel,<sup>1</sup> A. Bienfait,<sup>1,a)</sup> É. Dumur,<sup>1,2,b)</sup> H.-S. Chang,<sup>1</sup> M.-H. Chou,<sup>1,3</sup> C. R. Conner,<sup>1</sup> G. A. Peairs,<sup>1,4</sup> R. G. Povey,<sup>1,5</sup> Y. P. Zhong,<sup>1</sup> and A. N. Cleland<sup>1,2,c)</sup>

## AFFILIATIONS

<sup>1</sup>Pritzker School of Molecular Engineering, University of Chicago, Chicago, Illinois 60637, USA

<sup>2</sup>Institute for Molecular Engineering and Materials Science Division, Argonne National Laboratory, Lemont, Illinois 60439, USA

<sup>3</sup>Department of Physics, University of Chicago, Chicago, Illinois 60637, USA

<sup>4</sup>Department of Physics, University of California, Santa Barbara California 93106, USA

<sup>a)</sup>Present address: Université de Lyon, ENS de Lyon, Université Claude Bernard, CNRS, Laboratoire de Physique, F-69342 Lyon, France.

<sup>b)</sup>Present address: Université Grenoble Alpes, CEA, INAC-Phelq, QuantECA, 38000 Grenoble, France.

<sup>c)</sup>Author to whom correspondence should be addressed: [anc@uchicago.edu](mailto:anc@uchicago.edu)

## ABSTRACT

Broadband quantum-limited amplifiers play a critical role in the single-shot readout of superconducting qubits, but a popular implementation, the traveling wave parametric amplifier, involves a complex design and fabrication process. Here, we present a simple design for a Josephson parametric amplifier, using a lumped element resonator comprising a superconducting quantum interference device whose useful bandwidth is enhanced with an on-chip impedance-matching circuit. We demonstrate a flux-coupling geometry that maximizes the coupling to the Josephson loop and minimizes spurious excitation of the amplifier resonant circuit. The amplifier, which operates in a flux-pumped mode, is demonstrated with a power gain of more than 20 dB over a bandwidth of about 300 MHz, where approximate noise measurements indicate quantum-limited performance. A procedure is given for optimizing the bandwidth for this kind of amplifier, using a linearized circuit simulation while minimizing non-linearities.

Published under license by AIP Publishing. <https://doi.org/10.1063/5.0035945>

High-fidelity single-shot readout of superconducting qubits requires the lowest-noise amplification to achieve fast discrimination of the intrinsically small readout signals.<sup>1–3</sup> A popular approach is to use traveling wave parametric amplifiers (TWPAs),<sup>4–6</sup> which are broadband low-noise amplifiers approaching quantum-limited performance. Josephson parametric amplifiers (JPAs) provide similar or better noise performance compared to TWPAs<sup>2,7–11</sup> and, in addition, can operate as phase-sensitive amplifiers. Depending on the implementation, JPAs can also provide tunable operation with bandwidths exceeding 100 MHz with reasonable saturation powers. Here, we explore a number of innovations to improve the performance of a JPA that is simple to fabricate and simple to operate, affords quantum-limited noise amplification over a bandwidth of greater than 300 MHz, and operates in flux-pumped mode, separating the pump from the amplified signal and, thereby, making post-processing of the signal more straightforward.

The JPA is often viewed as a narrow-band amplifier because this device is typically designed as a nonlinear resonant cavity whose resonance width determines the useful amplifier bandwidth. TWPAs circumvent this bandwidth limitation by distributing the amplifying non-linearity over a transmission line.<sup>4</sup> Designs for JPAs that increase the amplification bandwidth while maintaining a simple fabrication process would provide a welcome addition to the Josephson amplifier family.<sup>12,13</sup>

A JPA can be designed to amplify signals with either a three-wave or four-wave mixing process, typically implemented using either current-pumping or flux-pumping, respectively.<sup>14</sup> Four-wave JPAs<sup>7</sup> operate with a pump tone  $\omega_p$  near the signal  $\omega_s$  and idler  $\omega_i$  frequencies, with  $2\omega_p = \omega_s + \omega_i$  and  $\omega_s \approx \omega_i$ , where amplification occurs through a fourth-order Kerr non-linearity in the circuit Hamiltonian. Three-wave JPAs<sup>9</sup> operate with a pump tone near twice the signal frequency,  $\omega_p = \omega_s + \omega_i$ , with amplification due to the frequency

modulation of a Josephson superconducting quantum interference device (SQUID) loop. The separation of the pump and signal tones removes the need for post-amplifier filtering circuitry.<sup>3</sup> Flux pumping with three-wave mixing can be performed with a pump line separated from the signal line, displacing the pump tone from the signal tone both physically and in frequency.

The achievable bandwidth for both four- and three-wave JPAs can be increased significantly, from tens of MHz in a basic design to hundreds of MHz by impedance-matching the amplifier to its input. This can be achieved by using an impedance-matching taper,<sup>15</sup> or, in a particularly simple version of this concept, using a series-connected  $\lambda/4$  and  $\lambda/2$  impedance transformer.<sup>13</sup> In the latter demonstration, the transformer was off-chip and the JPA was operated in four-wave mode.

Here, we extend the work of Ref. 13 using an on-chip impedance transformer and an improved flux coupling to the SQUID that enables flux pumping and both three- and four-wave amplification, with the entire device fabricated monolithically on a single die. The amplifier is operated in reflection, with the input signal reflected as an amplified output signal with a gain of more than 20 dB. This provides a simple design easily integrated with superconducting qubit circuitry. A galvanic connection to the input reduces the coupling quality factor, increasing the amplification bandwidth. A SQUID loop is formed with two Josephson junctions in parallel,<sup>16</sup> which when combined with an on-chip flux line, affords *in situ* tuning of the amplifier frequency and flux pumping. We use a symmetrically coupled on-chip flux line that minimizes spurious mode coupling, thereby enabling operation in a flux-pumped mode. We also use a via-free parallel plate capacitor design with a low-loss dielectric that provides an easily fabricated pF-range input capacitance. Numerical simulations are used to select device parameters that optimize the amplification bandwidth and minimize non-linearities.

Figure 1 shows images of an impedance-engineered JPA device and its equivalent circuit, fabricated on intrinsic ( $>10$  k $\Omega$  cm resistivity) silicon. The base wiring is etched from a uniformly evaporated film of 100 nm thick Al, patterned using a photoresist-masked  $\text{Cl}_2$  reactive ion etch process. A  $\lambda/4$  resonator centered at 5.3 GHz with a characteristic impedance of 45  $\Omega$  matches the 50  $\Omega$  impedance input line to 40  $\Omega$ , lowering the quality factor of the JPA resonance; the  $\lambda/2$  resonator with a characteristic impedance of 80  $\Omega$ , also centered at 5.3 GHz, reduces the frequency dependence in the system susceptibility matrix, thereby increasing the amplification bandwidth.<sup>13</sup> To prevent microwave-frequency slot modes, Al cross-overs with the same dielectric as the capacitor are placed on the impedance-matching resonators every 200  $\mu\text{m}$ .<sup>17</sup>

The input to the JPA itself includes a via-free parallel-plate capacitor with a total input capacitance of  $C = 2.03 \pm 0.02$  pF to ground. The impedance-transformed input line is galvanically connected to the bottom capacitor plate, which is, in turn, galvanically connected to the SQUID. The capacitor top electrode is formed by a 200 nm thick Al film on a 250 nm thick dielectric, and the dielectric is formed by 10 nm thick silicon nitride (SiN) layers on the top and bottom for improved film quality, with the remaining thickness comprising hydrogen-saturated amorphous silicon (*a*-Si), chosen for its low dielectric loss.<sup>18</sup> The top capacitor plate is capacitively coupled to ground, in parallel with the SQUID, and has no galvanic connections. The SQUID is formed by two identical Josephson junctions connected

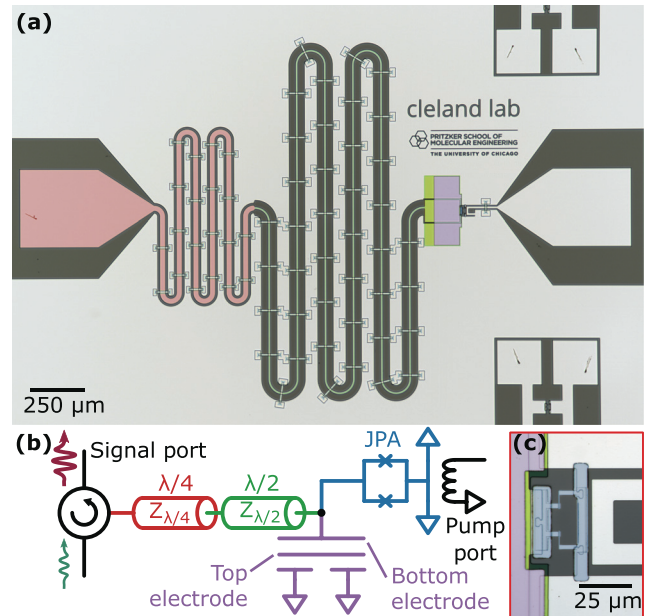


**FIG. 1.** Experimental device. (a) Micrograph of the fabricated device with a series  $\lambda/4$  transformer with impedance  $Z_{\lambda/4} = 45 \Omega$  (red), a  $\lambda/2$  transformer with impedance  $Z_{\lambda/2} = 80 \Omega$  (green), and a via-free parallel plate capacitor (purple). (b) Circuit representation of the device. (c) Higher-magnification micrograph of the JPA SQUID (blue) and its associated flux line.

in parallel, designed to have a combined critical current of 2.64  $\mu\text{A}$  and an enclosed loop area of 220  $\mu\text{m}^2$ . The SQUID and its flux-pumping line, shown in detail in Fig. 1(c), are designed to have mirror symmetry about the SQUID connection point to the capacitor base, thereby minimizing the coupling of microwave-frequency pump tones to spurious modes; the flux pumping line also includes a single grounded Al crossover.

Choosing the JPA parameters is a non-trivial optimization problem: An ideal JPA is designed to maximize its amplification bandwidth and saturation power, while minimizing added noise. Approximate analytic solutions can be used to guide simple device designs;<sup>21</sup> however, numerical simulations are more appropriate for simultaneously optimizing multiple parameters. We optimized using numerical simulations based on the pumpistator model,<sup>19,20</sup> where the SQUID, in the presence of a parametric flux pump, is modeled as a linear inductance combined with an effective negative resistance, as shown in Fig. 2(a). We note that this specific model for the SQUID is only valid for the three-wave non-degenerate mode of operation. The impedance-transforming input circuit is modeled using standard transmission-line equations. The SQUID inductances  $L_{n,0}$  and  $L_{n,2}$  are defined<sup>20</sup> as

$$L_{n,0} = L_J / \epsilon_0, \quad (1)$$

$$L_{n,2} = -\frac{L_J}{|\epsilon_1|^2} (\epsilon_0 - j\omega L_J Y_i^*), \quad (2)$$

where  $L_J = L_s / \cos(\pi\Phi_{\text{DC}})$ ,  $\epsilon_0 = 1 - (1/4)(\pi\Phi_{\text{AC}})^2$ , and  $\epsilon_1 = (\pi\Phi_{\text{AC}}/2) \tan(\pi\Phi_{\text{DC}})$ . These parameters are functions of the SQUID bare inductance  $L_s$ , the DC flux  $\Phi_{\text{DC}}$ , the AC flux amplitude

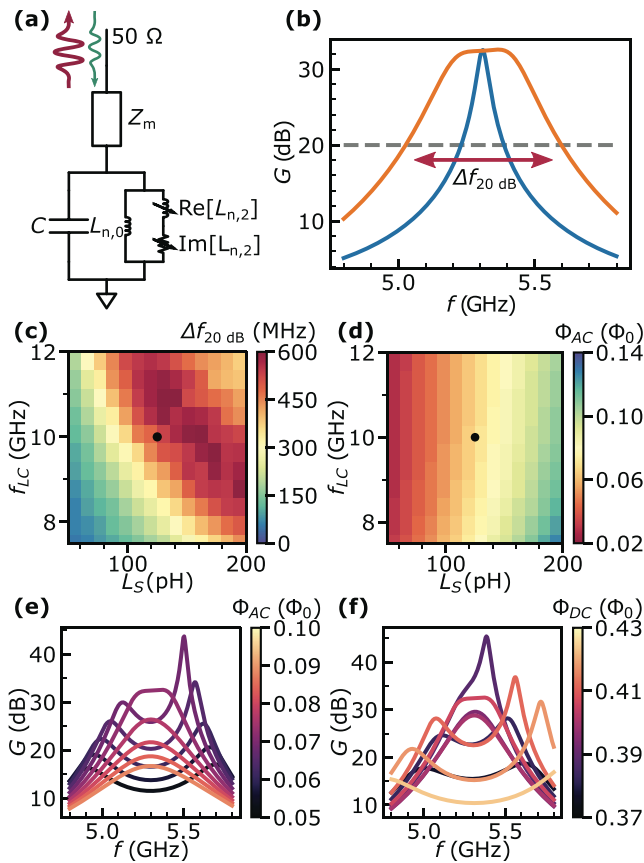


**FIG. 2.** JPA simulated power gain and bandwidth using the pumpistop model.<sup>19,20</sup> (a) Linearized circuit used for simulations with impedance-matching element  $Z_m$ , JPA capacitance  $C = 2.03$  pF, SQUID static inductance  $L_{n,0}$ , SQUID variable inductance  $\text{Re}[L_{n,2}]$ , and variable resistance (imaginary inductance)  $\text{Im}[L_{n,2}]$ . The variable circuit elements are functions of the pump amplitude  $\Phi_{AC}$  and the DC flux  $\Phi_{DC}$ , plotted in units of the flux quantum  $\Phi_0 = h/2e$  in panels (d)–(f). (b) Simulated power gain curve  $G(f)$  as a function of signal frequency  $f$  for a JPA circuit with (orange) and without (blue) the impedance-matching element  $Z_m$ . Red arrows indicate the bandwidth  $\Delta f_{20\text{dB}}$  for which the power gain is greater than 20 dB. (c) Bandwidth  $\Delta f_{20\text{dB}}$  and (d)  $\Phi_{AC}$  calculated for the optimized operating point as a function of the bare SQUID inductance  $L_s$  and bare LC resonance frequency  $f_{LC} = 1/(2\pi\sqrt{L_s C})$ . Black dots show design parameters for the fabricated device, where  $L_s = 125$  pH and  $f_{LC} = 10$  GHz. (e) Simulated gain curves with  $L_s = 125$  pH and  $f_{LC} = 10$  GHz, for different  $\Phi_{AC}$  values and (f)  $\Phi_{DC}$ , near the operating point where  $\Phi_{DC} = 0.41 \Phi_0$  and  $\Phi_{AC} = 0.073 \Phi_0$ .

$\Phi_{AC}$ , and the external admittance  $Y_i$  seen by the SQUID at the idler frequency  $\omega_i$ .

This allows us to model the JPA power gain  $G(f)$  as a function of frequency, shown for typical parameters in Fig. 2(b), both with and without the input impedance transformer. The transformer significantly increases the bandwidth  $\Delta f_{20\text{dB}}$  over which the gain is larger than 20 dB, as shown by the red arrow. We choose a 20 dB bandwidth because, at that gain, the noise contribution from typical cryogenic second-stage amplifiers can be neglected. In our setup, for example, we use a high-electron-mobility transistor (HEMT) amplifier with a noise temperatures of  $\sim 2$  K, which referenced to the JPA input that is

reduced to  $\sim 20$  mK for a gain of 20 dB,<sup>22</sup> contributing a small amount to the quantum-limited noise of  $hf/k_B = 240$  mK at  $f = 5$  GHz.

The response of the JPA depends critically on the SQUID design parameters. In Figs. 2(c) and 2(d), we show the bandwidth  $\Delta f_{20\text{dB}}$  (color scale) and the flux pump modulation amplitude  $\Phi_{AC}$ , calculated as a function of the SQUID linearized inductance  $L_s$  and the SQUID bare LC frequency  $f_{LC} = 1/(2\pi\sqrt{L_s C})$ . These are optimized at each operating frequency by first setting  $\Phi_{DC}$  to achieve a gain greater than 20 dB with minimal  $\Phi_{AC}$  and then varying  $\Phi_{AC}$  to maximize the bandwidth. When choosing device parameters, one might pick a SQUID inductance  $L_s$  to maximize the bandwidth; however, a practical JPA design should also minimize the pump amplitude  $\Phi_{AC}$  in order to reduce non-linearities in the pumping process. As seen in Figs. 2(c) and 2(d), these two criteria are in opposition; here, we compromise and chose device parameters that optimize the bandwidth while keeping the pump amplitude below  $0.1 \Phi_0$ , shown by the black dots in the panels, with  $L_s = 125$  pH and  $f_{LC} = 10$  GHz.

With fixed physical parameters  $L_s$  and  $f_{LC}$  the gain curve  $G(f)$  still depends on the flux-bias operating point  $\Phi_{DC}$  as well as the modulation amplitude  $\Phi_{AC}$  of the flux pump, as shown in Figs. 2(e) and 2(f).

The frequency and value of the maximum JPA gain also depend on the detailed input circuit.<sup>13,15</sup> We model the input line as an ideal  $50 \Omega$  impedance connected to the input impedance transformers. In a real device, the input would include non-ideal circulators, cables, and wire-bond connections, each modifying the gain-frequency  $G(f)$  response. Note that the impedance transformer can be chosen to yield large bandwidths in simulation, but JPA impedances below  $10 \Omega$  are difficult to optimally match to a  $50 \Omega$  input line impedance; furthermore, optimally matching these impedances increases the required flux modulation  $\Phi_{AC}$ . We chose impedance transformer parameters that are reasonable to fabricate and then optimized the JPA parameters given this fixed input circuit.

The device is operated on the mixing chamber plate of a dilution refrigerator with a base temperature of 7 mK. The signal is measured in reflection and then amplified using a commercial HEMT amplifier. With no AC flux pump, two resonances are visible as the DC flux is varied, shown in Fig. 3(a). These resonances match a linear circuit model including the  $\lambda/4$  and  $\lambda/2$  transmission lines loaded by a parallel lumped-element LC resonator, where the SQUID inductance is modeled by the flux-biased inductance  $L_J = L_s / \cos(\pi\Phi_{DC})$ . The model lumped-element capacitance  $C$  and inductance  $L_J$  are assumed to have their design values, and both impedance-matching transmission line resonator frequencies are taken to be 5.3 GHz. After solving numerically for the impedance of this model as a function of frequency, the resonance is defined<sup>23</sup> as the frequency at which the reactive input impedance is zero.

In Fig. 3(b), we display the power gain  $G(f)$  for various pump powers  $P$  (measured at the top of the cryostat), measured with  $\Phi_{DC} = 0.47 \Phi_0$ . A pump power of 4 dBm corresponds to  $\Phi_{AC} = 0.07 \Phi_0$ , assuming the known cable attenuation of  $-40$  dBm and using the SQUID's estimated DC mutual inductance with the flux line of 1.35 pH; the value of  $\Phi_{AC}$  is consistent with simulations. The bandwidth  $\Delta f_{20\text{dB}}$  is measured as a function  $\Phi_{DC}$  and pump power  $P$  for a pump frequency of 10.62 GHz [see Fig. 3(b)]. We choose values of  $\Phi_{DC}$  and  $P$  that minimize the JPA noise and maximize the bandwidth. Using the optimized parameters, we measure  $\Delta f_{20\text{dB}} = 305$  MHz [see Fig. 3(d)]. A 1 dB saturation power of  $-116$  dBm is

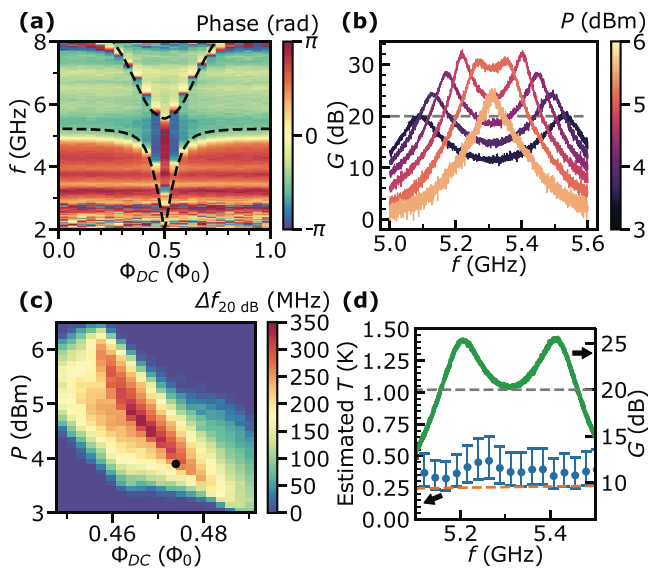


**FIG. 3.** Measured device performance, operated in a dilution refrigerator at 7 mK. (a) Phase of the small signal reflected from the amplifier as a function of frequency  $f$  and DC flux  $\Phi_{DC}$ . Dashed lines indicate resonances in a linear circuit model of the device without flux pumping. (b) Power gain  $G(f)$  as a function of frequency for various signal generator powers  $P$  at  $\Phi_{DC} = 0.47\Phi_0$ . (c) Bandwidth  $\Delta f_{20dB}$  as a function of pump power  $P$  and DC flux  $\Phi_{DC}$ . (d) Measured gain  $G(f)$  (green) and estimated noise temperature (blue) vs frequency  $f$  at the labeled point in panel c, displaying a bandwidth of 300 MHz. The noise quantum limit (orange) is given by  $T_N = hf/k_B$ . Noise temperature error bars are dominated by uncertainty in effective HEMT noise temperature.

measured for these operating parameters, which is similar to other lumped-element amplifiers.<sup>12</sup>

The noise temperature is roughly estimated using the HEMT as a calibration source [Fig. 3(d)], by comparing the signal-to-noise ratio for a weak signal while flux pumping the JPA to that without flux pumping. The amplification chain includes the JPA, attenuating elements following the JPA, and then the cryogenic HEMT amplifier. Circulators, cables, and connections between components are estimated to attenuate the signal between the JPA and HEMT by approximately  $2.6 \pm 1.5$  dB. The noise temperatures for the HEMT and JPA are then calculated by dividing the noise of each element  $N_i$  by  $k_B B$ , where  $B = 3$  MHz is the measurement bandwidth. This assumes that the JPA has unity gain when off, and that the JPA when on, and the HEMT gain, which are both much larger than 1. The estimated JPA noise temperature is consistent with near-quantum-limited operation.

In summary, we have demonstrated a simple impedance-matched Josephson parametric amplifier with an on-chip impedance transforming circuit that we operate in a three-wave (flux-pumped) mixing mode, yielding a simple monolithic device with the pump separated from the signal. The amplifier displays a large operating bandwidth of greater than 300 MHz with good noise performance. This device has also been measured in a four-wave (current-pumped) mixing mode with an operating bandwidth of 200 MHz with an average noise of 460 mK over its operating bandwidth. While here we report on a single device, similar performance has been measured in other devices with similar design parameters. The straightforward design and fabrication of this device make it more accessible to a wider

range of researchers who need a robust and simple broadband near-quantum-limited amplifier for microwave measurements.

We thank P. J. Duda for helpful discussions. Devices and experiments were supported by the Army Research Laboratory. É.D. was supported by LDRD funds from the Argonne National Laboratory; A.N.C. was supported in part by the DOE, Office of Basic Energy Sciences. This work was partially supported by the UChicago MRSEC (No. NSF DMR-2011854) and made use of the Pritzker Nanofabrication Facility, which receives support from SHyNE, a node of the National Science Foundation's National Nanotechnology Coordinated Infrastructure (No. NSF ECCS-2025633), with additional support from NSF (NSF award QLCI-HQAN 2016136). The authors declare no competing financial interest.

#### DATA AVAILABILITY

The data that support the findings of this study are available from the corresponding author upon reasonable request.

#### REFERENCES

- A. A. Clerk, M. H. Devoret, S. M. Girvin, F. Marquardt, and R. J. Schoelkopf, "Introduction to quantum noise, measurement, and amplification," *Rev. Mod. Phys.* **82**, 1155–1208 (2010).
- R. Vijay, D. H. Slichter, and I. Siddiqi, "Observation of quantum jumps in a superconducting artificial atom," *Phys. Rev. Lett.* **106**, 110502 (2011).
- P. Krantz, M. Kjaergaard, F. Yan, T. P. Orlando, S. Gustavsson, and W. D. Oliver, "A quantum engineer's guide to superconducting qubits," *Appl. Phys. Rev.* **6**, 021318 (2019).
- C. Macklin, K. O'Brien, D. Hover, M. E. Schwartz, V. Bolkhovskoy, X. Zhang, W. D. Oliver, and I. Siddiqi, "A near-quantum-limited Josephson traveling-wave parametric amplifier," *Science* **350**, 307–310 (2015).
- T. C. White, J. Y. Mutus, I.-C. Hoi, R. Barends, B. Campbell, Y. Chen, Z. Chen, B. Chiaro, A. Dunsworth, E. Jeffrey, J. Kelly, A. Megrant, C. Neill, P. J. J. O'Malley, P. Roushan, D. Sank, A. Vainsencher, J. Wenner, S. Chaudhuri, J. Gao, and J. M. Martinis, "Traveling wave parametric amplifier with Josephson junctions using minimal resonator phase matching," *Appl. Phys. Lett.* **106**, 242601 (2015).
- L. Planat, A. Ranadive, R. Dassonneville, J. Puertas Martínez, S. Léger, C. Naud, O. Buisson, W. Hasch-Guichard, D. M. Basko, and N. Roch, "Photonic-crystal Josephson traveling-wave parametric amplifier," *Phys. Rev. X* **10**, 021021 (2020).
- B. Yurke, L. R. Corruccini, P. G. Kaminsky, L. W. Rupp, A. D. Smith, A. H. Silver, R. W. Simon, and E. A. Whittaker, "Observation of parametric amplification and deamplification in a Josephson parametric amplifier," *Phys. Rev. A* **39**, 2519–2533 (1989).
- I. Siddiqi, R. Vijay, F. Pierre, C. M. Wilson, M. Metcalfe, C. Rigetti, L. Frunzio, and M. H. Devoret, "RF-driven Josephson bifurcation amplifier for quantum measurement," *Phys. Rev. Lett.* **93**, 207002 (2004).
- M. A. Castellanos-Beltran and K. W. Lehnert, "Widely tunable parametric amplifier based on a superconducting quantum interference device array resonator," *Appl. Phys. Lett.* **91**, 083509 (2007).
- T. Yamamoto, K. Inomata, M. Watanabe, K. Matsuba, T. Miyazaki, W. D. Oliver, Y. Nakamura, and J. S. Tsai, "Flux-driven Josephson parametric amplifier," *Appl. Phys. Lett.* **93**, 042510 (2008).
- N. Bergeal, F. Schackert, M. Metcalfe, R. Vijay, V. E. Manucharyan, L. Frunzio, D. E. Prober, R. J. Schoelkopf, S. M. Girvin, and M. H. Devoret, "Phase-preserving amplification near the quantum limit with a Josephson ring modulator," *Nature* **465**, 64–68 (2010).
- J. Y. Mutus, T. C. White, E. Jeffrey, D. Sank, R. Barends, J. Bochmann, Y. Chen, Z. Chen, B. Chiaro, A. Dunsworth, J. Kelly, A. Megrant, C. Neill, P. J. J. O'Malley, P. Roushan, A. Vainsencher, J. Wenner, I. Siddiqi, R. Vijay, A. N. Cleland, and J. M. Martinis, "Design and characterization of a lumped element single-ended superconducting microwave parametric amplifier with on-chip flux bias line," *Appl. Phys. Lett.* **103**, 122602 (2013).

- <sup>13</sup>T. Roy, S. Kundu, M. Chand, A. M. Vadiraj, A. Ranadive, N. Nehra, M. P. Patankar, J. Aumentado, A. A. Clerk, and R. Vijay, "Broadband parametric amplification with impedance engineering: Beyond the gain-bandwidth product," *Appl. Phys. Lett.* **107**, 262601 (2015).
- <sup>14</sup>S. Boutin, D. M. Toyli, A. V. Venkatramani, A. W. Eddins, I. Siddiqi, and A. Blais, "Effect of higher-order nonlinearities on amplification and squeezing in Josephson parametric amplifiers," *Phys. Rev. Appl.* **8**, 054030 (2017).
- <sup>15</sup>J. Y. Mutus, T. C. White, R. Barends, Y. Chen, Z. Chen, B. Chiaro, A. Dunsworth, E. Jeffrey, J. Kelly, A. Megrant, C. Neill, P. J. J. O'Malley, P. Roushan, D. Sank, A. Vainsencher, J. Wenner, K. M. Sundqvist, A. N. Cleland, and J. M. Martinis, "Strong environmental coupling in a Josephson parametric amplifier," *Appl. Phys. Lett.* **104**, 263513 (2014).
- <sup>16</sup>C. D. Tesche and J. Clarke, "Dc squid-noise and optimization," *J. Low Temp. Phys.* **29**, 301–331 (1977).
- <sup>17</sup>G. E. Ponchak, J. Papapolymerou, and M. M. Tentzeris, "Excitation of coupled slotline mode in finite-ground CPW with unequal ground-plane widths," *IEEE Trans. Microwave Theory Tech.* **53**, 713–717 (2005).
- <sup>18</sup>A. D. O'Connell, M. Ansmann, R. C. Bialczak, M. Hofheinz, N. Katz, E. Lucero, C. McKenney, M. Neeley, H. Wang, E. M. Weig, A. N. Cleland, and J. M. Martinis, "Microwave dielectric loss at single photon energies and millikelvin temperatures," *Appl. Phys. Lett.* **92**, 112903 (2008).
- <sup>19</sup>K. M. Sundqvist, S. Kintaş, M. Simoen, P. Krantz, M. Sandberg, C. M. Wilson, and P. Delsing, "The pumpistor: A linearized model of a flux-pumped superconducting quantum interference device for use as a negative-resistance parametric amplifier," *Appl. Phys. Lett.* **103**, 102603 (2013).
- <sup>20</sup>K. M. Sundqvist and P. Delsing, "Negative-resistance models for parametrically flux-pumped superconducting quantum interference devices," *EPJ Quantum Technol.* **1**, 6 (2014).
- <sup>21</sup>C. Eichler and A. Wallraff, "Controlling the dynamic range of a Josephson parametric amplifier," *EPJ Quantum Technol.* **1**, 2 (2014).
- <sup>22</sup>H. T. Friis, "Noise figures of radio receivers," *Proc. IRE* **32**, 419–422 (1944).
- <sup>23</sup>S. E. Nigg, H. Paik, B. Vlastakis, G. Kirchmair, S. Shankar, L. Frunzio, M. H. Devoret, R. J. Schoelkopf, and S. M. Girvin, "Black-box superconducting circuit quantization," *Phys. Rev. Lett.* **108**, 240502 (2012).